Simulation of Chemical Isomerization Reaction Dynamics on a NMR Quantum Simulator

Dawei Lu,[1] Nanyang Xu,[1] Ruixue Xu,[1] Hongwei Chen,[1] Jiangbin Gong,[2,3] Xinhua Peng,[1] and Jiangfeng Du[1,*]

[1]*Hefei National Laboratory for Physical Sciences at Microscale and Department of Modern Physics, University of Science and Technology of China, Hefei, Anhui, 230026, China*

[2]*Department of Physics and Centre for Computational Science and Engineering, National University of Singapore, Singapore 117542, Republic of Singapore*

[3]*NUS Graduate School for Integrative Sciences and Engineering, Singapore 117597, Republic of Singapore*

(Received 13 May 2011)

Quantum simulation can beat current classical computers with minimally a few tens of qubits. Here we report an experimental demonstration that a small nuclear-magnetic-resonance ~~(NMR)~~ quantum simulator is already able to simulate the dynamics of a prototype laser-driven isomerization reaction using engineered quantum control pulses. The experimental results agree well with classical simulations. We conclude that the quantum simulation of chemical reaction dynamics not computable on current classical computers is feasible in the near future.

DOI: PACS numbers: 03.67.Ac, 07.57.Pt, 42.50.Dv, 76.60.−k

Introduction.—In addition to offering general-purpose quantum algorithms with substantial speed-ups over classical algorithms [1] (e.g., Shor's quantum factorizing algorithm [2]), a quantum computer can be used to simulate specific quantum systems with high efficiency [3]. This quantum simulation idea was first conceived by Feynman [4]. Lloyd proved that with quantum computation architecture, the required resource for quantum simulation scales polynomially with the size of the simulated system [5], as compared with the exponential scaling on classical computers. During the past years several quantum simulation algorithms designed for individual problems were proposed [6–10], and ~~a~~ part of them have been realized using physical systems such as NMR [11–13] or trapped-ions [14]. For quantum chemistry problems,

ACC. CODE **LE13229** AUTHOR **LU**

Aspuru-Guzik *et al.* and Kassal *et al.* proposed quantum simulation algorithms to calculate stationary molecular properties [15] as well as chemical reaction rates [16], with the quantum simulation of the former experimentally implemented on both photonic quantum simulators [17] and NMR systems [18]. In this work we aim at the quantum simulation of the more challenging side of quantum chemistry problems—chemical reaction dynamics, presenting an experimental NMR implementation for the first time.

Theoretical calculations of chemical reaction dynamics play an important role in understanding reaction mechanisms and in guiding the control of chemical reactions [19,20]. On classical computers the computational cost for propagating the Schrödinger equation increases exponentially with the system size. Indeed, standard methods in studies of chemical reaction dynamics so far have dealt with up to 9 degrees of freedom (~~DOF~~d.o.f.) [21]. Some highly sophisticated approaches, such as the ~~multi-configurational~~multiconfigurational time-dependent Hartree ~~(MCTDH)~~ method [22], can treat dozens of ~~DOF~~d.o.f., but various approximations are necessary. So generally speaking, classical computers are unable to perform dynamical simulations for large molecules. For example, for a 10 ~~DOF~~d.o.f. system and if only 8 grid points are needed for the coordinate representation of each ~~DOF~~d.o.f., classical computation will have to store and operate 8^{10} data points, already a formidable task for current classical computers. ~~By~~In contrast, such a system size is manageable by a quantum computer with only 30 qubits.

In this Letter we demonstrate that the quantum dynamics of a laser-driven isomerization model reaction can be simulated by a small NMR system under quantum control pulses. Given the limited number of qubits, the potential energy curve is modeled by 8 grid points. The continuous reactant-to-product transformation observed in our quantum simulator is in remarkable agreement with a classical computation also based ~~also~~ upon an ~~8~~eight-dimensional Hilbert space. To our knowledge, this is the first explicit implementation of the quantum simulation of a chemical reaction process. Theoretical methods and general experimental techniques described in this work should motivate next-generation simulations of chemical reaction dynamics using a larger number of qubits as well as error-correction techniques [23].

Theory.—Previously we were able to simulate the ground-state energy of a ~~H~~hydrogen molecule [18]. Here, to simulate chemical reaction dynamics, we consider a one-dimensional model of a laser-driven isomerization reaction [24], namely, the hydrogen-transfer reaction of nonsymmetric substituted malonaldehydes, depicted in Fig. 1(a). The system Hamiltonian in the presence of an external laser field is given by

$$H(t) = T + V + E(t) \quad \text{with} \quad E(t) = -\mu\varepsilon(t). \tag{1}$$

In Eq. (1), $E(t)$ is the laser-molecule interaction Hamiltonian, $\mu = eq$ is the dipole moment operator, $\varepsilon(t)$ represents the driving electric field, $T = p^2/2m$ is the kinetic energy operator, and

$$V = \frac{\Delta}{2q_0}(q - q_0) + \frac{V^{\ddagger} - \Delta/2}{q_0^4}(q - q_0)^2(q + q_0)^2 \tag{2}$$

is a double-well potential of the system along the reaction coordinate. In Eq. (2) $V^{\ddagger}$ is the barrier height, Δ

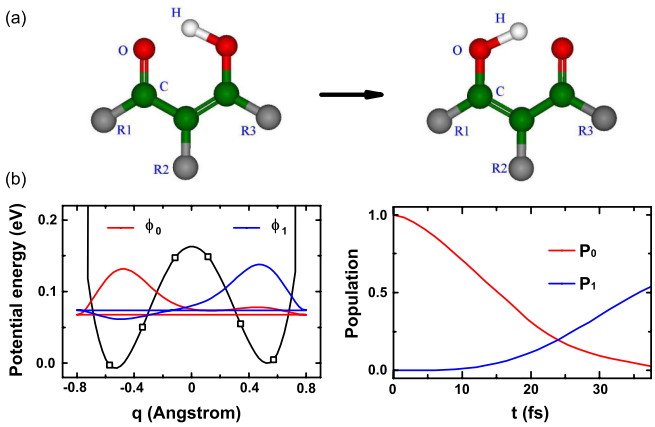

FIG. 1 (color online). (a) Isomerization reaction of nonsymmetric substituted malonaldehydes. (b) Left panel: Potential energy curve, together with the eigenfunctions of the ground (red) and the first excited (blue) states. The main system parameters [Eq. (2)] are taken from Ref. [24], with $V^{\ddagger} = 0.006\,25E_h$, $\Delta = 0.000\,257E_h$, and $q_0 = 1a_0$. The potential values for q approaching the left and right ends are increased to obtain rapid decay of wave_function amplitudes. Right panel: Numerically exact time-dependence of populations of the ground state (reactant state, denoted P_0) and the first excited state (product state, denoted P_1).

gives the asymmetry of the two wells, and $\pm q_0$ give the locations of the potential well minima. See the ~~figure~~ caption of Fig. 1(b) for more details of this model.

We first employ the split-operator method [16,25] to obtain the propagator $U(t + \delta t, t)$ associated with the time interval from t to $t + \delta t$. We then have

$$U(t + \delta t, t) \approx e^{-(i/\hbar)(V\delta t/2)} e^{-(i/\hbar)[E(t+\delta t/2)\delta t/2]} e^{-(i/\hbar)T\delta t} e^{-(i/\hbar)[E(t+\delta t/2)\delta t/2]} e^{-(i/\hbar)(V\delta t/2)}. \tag{3}$$

The unitary operator $e^{-iT\delta t/\hbar}$ in Eq. (3) is diagonal in the momentum representation whereas all the other operators are unitary and diagonal in the coordinate representation. Such $U(t + \delta t, t)$ can be simulated in a rather simple fashion if we work with both representations and make transformations between them by quantum Fourier transform (QFT) operations. To take snapshots of the dynamics we divide the reaction process into 25 small time steps, with $\delta t = 1.5$ fs and the total duration $t_f = 37.5$ fs. The electric field of an ultrashort strong laser pulse is chosen as

$$\varepsilon(t) = \begin{cases} \varepsilon_0 \sin^2(\frac{\pi t}{2s_1}) & 0 \le t \le s_1 \\ \varepsilon_0 & s_1 < t < s_2 \\ \varepsilon_0 \sin^2[\frac{\pi(t_f - t)}{2(t_f - s_2)}] & s_2 \le t \le t_f, \end{cases} \tag{4}$$

with $s_1 = 5$ fs and $s_2 = 32.5$ fs. More details, including an error analysis of the split-operator technique, are given in the supplementary material [26]. The reactant state at $t = 0$ is assumed to be the ground-state $|\phi_0\rangle$ of the bare Hamiltonian $T + V$, which is mainly localized in the left potential well. The wave function of the reacting system at later times is denoted by $|\psi(t)\rangle$. The product state of the reaction is taken as the first excited state $|\phi_1\rangle$ of $T + V$, which is mainly localized in the right potential well.

With the system Hamiltonian, the initial reactant state, the product state, and the propagation method outlined above, the next step is to encode the time-evolving wave function $|\psi(t)\rangle$ and the T, V, $E(t)$ operators by n qubits. To that end we first obtain the expressions of these operators in representation of a set of $N = 2^n$ discretized position basis states. The evolving state can then be encoded as

$$|\psi(t)\rangle = \sum_{q=0}^{2^n-1} m_q(t)|q\rangle = m_0(t)|0\cdots00\rangle + \cdots + m_{2^n-1}(t)|1\cdots11\rangle. \tag{5}$$

Because our current quantum simulation platform can only offer a limited number of qubits and the focus of this work is on an implementation of the necessary gate operations under the above encoding, we have

employed a rather aggressive ~~8~~eight-point discretization using $n = 3$ qubits. The associated diagonal forms of the T, V, and q matrices are given in the supplementary material [26]. In particular, the end grid points are at $q = \pm 0.8$ Å and the locations of other ~~6~~six grid points are shown in Fig. 1(b). The eigenvalues of the ground and first excited states of the bare Hamiltonian treated in the ~~8~~eight-dimensional encoding Hilbert space are close to the exact answers. The associated eigenfunctions are somewhat deformed from exact calculations using, e.g., 64 grid points. Nonetheless, their unbalanced probability distribution in the two potential wells is maintained. For example, the probability for the first excited state being found in the right potential well is about 80%.

Experiment.—In our experiment qubits 1, 2, and 3 are realized by the ^{19}F, ^{13}C, and ^{1}H nuclear spins of Diethyl-fluoromalonate. The structure of Diethyl-fluoromalonate is shown in Fig. 2(a), where the three nuclei used as qubits are marked by the oval. The internal Hamiltonian of this system is given by

$$\mathcal{H}_{\text{int}} = \sum_{j=1}^{3} 2\pi\nu_j I_z^j + \sum_{j<k,=1}^{3} 2\pi J_{jk} I_z^j I_z^k, \tag{6}$$

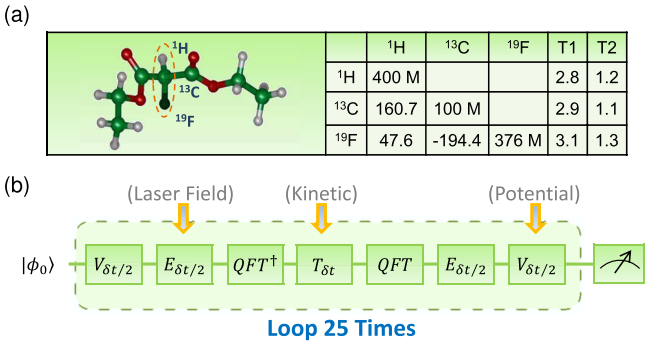

	^{1}H	^{13}C	^{19}F	T1	T2
^{1}H	400 M			2.8	1.2
^{13}C	160.7	100 M		2.9	1.1
^{19}F	47.6	-194.4	376 M	3.1	1.3

FIG. 2 (color online). (a) Molecular structure of Diethyl-fluoromalonate and the system parameters. The ^{1}H, ^{13}C, and ^{19}F nuclear spins marked by the oval are used as ~~three~~3 qubits. Diagonal elements are the Larmor frequencies (Hz), and off-diagonal elements are scalar coupling strength (Hz) between two nuclear spins. Relaxation and dephasing time scales (second) T_1 and T_2 for each nuclear spin are listed on the right. (b) The network of quantum operations to simulate the isomerization dynamics, with the reactant state $|\phi_0\rangle$. The whole process is divided into 25 loops. The operators $T_{\delta t}$, $V_{\delta t}$, and $E_{\delta t/2}$ are assumed to be in their diagonal representations.

where ν_j is the resonance frequency of the jth spin and J_{jk} is the scalar coupling strength between spins j and k. The experiment is conducted on a Bruker Avance 400 MHz spectrometer at room temperature.

The experiment consists of three parts: (A) Initial state preparation. In this part we prepare the ground state $|\phi_0\rangle$ of the bare Hamiltonian $T + V$ as the reactant state. (B) Dynamical evolution, that is, the explicit implementation of the system evolution such that the continuous chemical dynamics can be simulated. (C) Measurement. In this third part the probabilities of the reactant and product states associated with each of the 25 snapshots of the dynamical evolution are recorded. For the jth snapshot at $t_j \equiv j\delta t$, we measure the

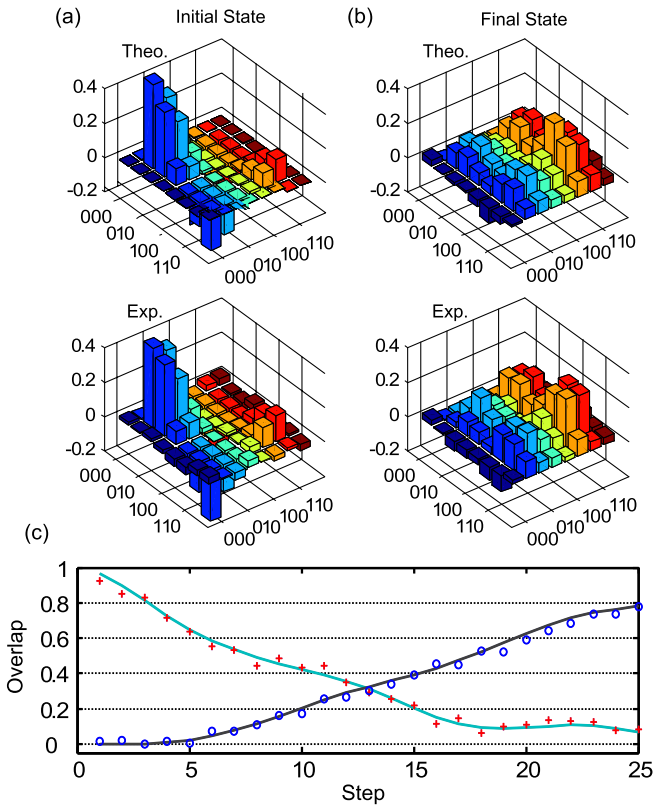

FIG. 3 (color online). (a)–(b) Real part of the density matrix of the initial and final states of the simulated reaction. Upper panels show the theoretical results based on an eight-dimensional Hilbert space, and lower panels show the experimental results. (c) The measured probabilities of the reactant and product states to give 25 snapshots of the reaction dynamics. The (red) plus symbols represent measured results of $C(|\psi(t_j)\rangle, |\phi_0\rangle)$ and the (blue) circles represent measured results of $C(|\psi(t_j)\rangle, |\phi_1\rangle)$, both in agreement with the theoretical smooth curves. Results here also agree qualitatively with the numerically exact dynamics shown in Fig. 1(b).

overlaps $C(|\psi(t_j)\rangle, |\phi_0\rangle) = |\langle\phi_0|\psi(t_j)\rangle|^2$ and $C(|\psi(t_j)\rangle, |\phi_1\rangle) = |\langle\phi_1|\psi(t_j)\rangle|^2$, through which the continuous reactant-to-product transformation can be displayed. The main experimental details are as follows. Readers may again refer to the supplementary material [26] for more technical explanations.

(A) Initial ~~S~~state ~~P~~preparation: Starting from the thermal equilibrium state, first~~ly~~ we create the ~~pseudo-pure~~pseudopure state ~~(PPS)~~ $\rho_{000} = (1-\epsilon)\mathbb{I}/8 + \epsilon|000\rangle\langle 000|$ using the spatial average technique [27], where $\epsilon \approx 10^{-5}$ represents the polarization of the system and $\mathbb{I}$ is the 8×8 identity matrix. The initial state $|\phi_0\rangle$ was prepared from ρ_{000} by applying one shaped radio-frequency (~~RF~~rf) pulse characterized by 1000 frequency segments and determined by the ~~GR~~gradient ~~A~~ascent ~~P~~pulse ~~E~~engineering (GRAPE) algorithm [28–30]. The preparation pulse is obtained with the pulse width chosen as 10 ms and a theoretical fidelity 0.995. To confirm the successful preparation of the state $|\phi_0\rangle$, we carry out a full state tomography and examine the fidelity between the target density matrix $\rho_0 = |\phi_0\rangle\langle\phi_0|$ and the experimental one $\rho_{\text{expt}}(0)$ ~~$\rho_{\text{exp}}(0)$~~ . Using the fidelity definition $F(\rho_1, \rho_2) \equiv \text{Tr}(\rho_1\rho_2)/\sqrt{(\text{Tr}(\rho_1^2)\,\text{Tr}(\rho_2^2)}$, we obtain $F[\rho_0, \rho_{\text{expt}}(0)] = 0.950$ ~~$F[\rho_0, \rho_{\text{exp}}(0)] = 0.950$~~ . Indeed, their real parts shown in Fig. 3(a) are seen to be in agreement.

(B) Dynamical ~~E~~evolution: The reaction process was divided into $M = 25$ discrete time intervals of the same duration δt. Associated with the mth time interval, the unitary evolution operator is given by

$$U_m \approx V_{\delta t/2} E_{\delta t/2}(t_m) U_{\text{QFT}} T_{\delta t} U_{\text{QFT}}^{\dagger} E_{\delta t/2}(t_m) V_{\delta t/2}, \tag{7}$$

where U_{QFT} represents a QFT operation, and other operators are defined by $V_{\delta t/2} \equiv e^{-(i/\hbar)V(\delta t/2)}$, $T_{\delta t} \equiv e^{-(i/\hbar)T\delta t}$, and $E_{\delta t/2}(t_m) \equiv e^{(i/\hbar)\varepsilon(t_{m-1}+\delta t/2)eq(\delta t/2)}$, with V, T, and q all in their diagonal representations. Such a loop of operations is m-dependent because the simulated system is subject to a time-dependent laser field.

Each individual operation in the U_m loop can be implemented by a particular ~~RF~~rf pulse sequence applied to our system. However, in the experiment such a direct decomposition of U_m requires a very long gate operation time and highly complicated ~~RF~~rf pulse sequences. This bottom-up approach hence accumulates considerable experimental errors and also invites serious decoherence effects. To circumvent this technical

problem we find an alternative experimental approach, which further exploits the GRAPE technique to synthesize U_m or their products with one single engineered ~~RF~~rf pulse only. That is, the quantum evolution operator $U(t_j, 0)$, which is simulated by $\prod_{m=1}^{j} U_m$, is implemented by one GRAPE coherent control pulse altogether, with a preset fidelity and a typical pulse length ranging from 10 ~~ms~~ to 15 ms. For the 25 snapshots of the dynamics, totally 25 ~~GRAPE~~GRAPE pulses are worked out, with their fidelities always set to be larger than 0.99. As a result, the technical complexity of the experiment decreases dramatically, the error accumulation due to gate imperfections is avoided, and the simulation fidelity is maintained at a high level. The task of finding a ~~GRAPE~~GRAPE pulse itself may be fulfilled via feedback learning control [19] that can exploit the quantum evolution of our NMR system itself. However, this quantum procedure is not essential or necessary in our experiment because here the ~~GRAPE~~GRAPE pulses on a 3-qubit system can be found rather easily.

(C) Measurement: To take the snapshots of the reaction process at $t_j = j\delta t$ we need to measure the overlaps of $C(|\psi(t_j)\rangle, |\phi_0\rangle)$ and $C(|\psi(t_j)\rangle, |\phi_1\rangle)$. A full state tomography at t_j will do, but this will produce much more information than needed. Indeed, assisted by a simple diagonalization technique, sole population measurements already suffice to observe the reactant-to-product transformation (~~S~~see the supplementary material [26]).

To assess the difference between theory and experiment, we carry out one full state tomography for the final state density matrix at $t = t_f$. Because the GRAPE pulse is made to reach a fidelity larger than 0.995, the experimental density matrix $\rho_{\text{expt}}(t_f)$ ~~$\rho_{\text{exp}}(t_f)$~~ is indeed very close to the theoretical density matrix $\rho_{\text{theor}}(t_f)$ ~~$\rho_{\text{theory}}(t_f)$~~ obtained in an ~~8~~eight-dimensional Hilbert space, with a fidelity $F[\rho_{\text{theor}}(t_f), \rho_{\text{expt}}(t_f)] = 0.957$ ~~$F[\rho_{\text{theory}}(t_f), \rho_{\text{exp}}(t_f)] = 0.957$~~. The experimental density matrix elements of the final state shown in Fig. 3(b) match the theoretical results to a high degree. With confidence in the experimental results on the full density matrix level, we can now examine the simulated reaction dynamics, reporting only the probabilities of the reactant and product states. Figure 3(c) shows the time- dependence of the probabilities of both the reactant and product states obtained from our quantum

simulator. It is seen that the product-to-reactant ratio increases continuously with time, with the probability of the product state reaching 77% at the end of the simulated reaction. A prototype laser-driven reaction is thus successfully simulated by our 3-qubit system. We emphasize that due to the use of GRAPE pulses in synthesizing the gate operations, our simulation experiment lasts about 30 ms only, which is much shorter than the spin decoherence time of our system. The slight difference between theory and experiment can be attributed to imperfect GRAPE pulses, as well as inhomogeneity in ~~RF~~rf pulses and in the static magnetic field.

Conclusion.—A quantum simulator attacking problems not solvable on current classical computers will be one conceivable milestone in the very near future. The realization of quantum simulations will tremendously change the way we explore quantum chemistry in both stationary and dynamical problems [15,16]. Our work reported here is the first experimental study of the quantum simulation of a prototype laser-driven chemical reaction. This is made possible by shaped quantum control pulses that do not accumulate errors due to gate imperfections. Our proof-of-principle experiment also realizes a promising map from laser-driven chemical reactions to the dynamics of interacting spin systems under shaped ~~RF~~rf fields, thus bridging ~~up~~ two research subjects whose characteristic time scales differ by many orders of magnitude.Acknowledgments

Helpful discussions with J. L. Yang are gratefully acknowledged. This work was supported by National Nature Science Foundation of China, the CAS, and the National Fundamental Research Program 2007CB925200.

*djf@ustc.edu.cn

[1] M. A. Nielson and I. L. Chuang, *Quantum Computation and Quantum Information* (Cambridge Univ.ersity Press, Cambridge, ~~U. K.~~England, 2000).

[2] P. Shor, in *Proceedings of the 35th Annual Symposium on Foundations of Computer Science, Santa Fe, NM, 1994* (IEEE, New York, 1994), p. 124.

[3] I. Buluta and F. Nori, Science **326**, 108 (2009).

[4] R. P. Feynman, Int. J. Theor. Phys. **21**, 467 (1982).

[5] S. Lloyd, Science **273**, 1073 (1996).

[6] C. Zalka, in *Proceedings of the ITP Conference on Quantum Coherence and Decoherence, Santa Barbara, CA, 1996* (Royal Society London, London, 1996), pp. 313–322.

[7] D. S. Abrams and S. Lloyd, Phys. Rev. Lett. **79**, 2586 (1997).

[8] L. A. Wu, M. S. Byrd, and D. A. Lidar, Phys. Rev. Lett. **89**, 057904 (2002).

[9] A. Y. Smirnov *et al.*, Europhys. Lett. **80**, 67008 (2007).

[10] D. A. Lidar and H. Wang, Phys. Rev. E **59**, 2429 (1999).

[11] X. H. Peng, J. F. Du, and D. Suter, Phys. Rev. A **71**, 012307 (2005).

[12] S. Somaroo *et al.*, Phys. Rev. Lett. **82**, 5381 (1999).

[13] C. Negrevergne *et al.*, Phys. Rev. A **71**, 032344 (2005).

[14] A. Friedenauer *et al.*, Nature Phys. **4**, 757 (2008).

[15] A. Aspuru-Guzik *et al.*, Science **309**, 1704 (2005).

[16] I. Kassal *et al.*, Proc. Natl. Acad. Sci. U.S.A. **105**, 18 681 (2008).

[17] B. P. Lanyon *et al.*, Nature Chem. **2**, 106 (2010).

[18] J. F. Du *et al.*, Phys. Rev. Lett. **104**, 030502 (2010).

[19] H. Rabitz *et al.*, Science **288**, 824 (2000); W. S. Warren, H. Rabitz, and M. Dahleh, Science **259**, 1581 (1993).

[20] S. A. Rice and M. Zhao, *Optical Control of Molecular Dynamics* (John Wiley, New York, 2000); M. Shapiro and P. Brumer, *Principles of the Quantum Control of Molecular Processes* (John Wiley, New York, 2003).

[21] D. Wang, J. Chem. Phys. **124**, 201105 (2006).

[22] H.-D. Meyer and G. A. Worth, Theor. Chem. Acc. **109**, 251 (2003).

[23] K. R. Brown, R. J. Clark, and I. L. Chuang, Phys. Rev. Lett. **97**, 050504 (2006).

[24] N. Došlić *et al.*, J. Phys. Chem. A **102**, 9645 (1998).

[25] C. Zalka, Proc. R. Soc. A **454**, 313 (1998); S. Wiesner, arXiv:quant-ph/9603028.

[26] See supplemental material at http://link.aps.org/supplemental/10.1103/PhysRevLett.000.000000 for [brief description].

[27] D. G. Cory, A. F. Fahmy, and T. F. Havel, Proc. Natl. Acad. Sci. U.S.A. **94**, 1634 (1997).

[28] N. Khaneja *et al.*, J. Magn. Reson. **172**, 296 (2005).

[29] J. Baugh *et al.*, Phys. Canada **63**, 4 (2007).

[30] C. A. Ryan *et al.*, Phys. Rev. A **78**, 012328 (2008).